New Methanofullerenes Containing Amide as Electron Acceptor for Construction Photovoltaic Devices

Chao Liu,[†,‡] Yongjun Li,[*,†] Cuihong Li,[†] Weiwei Li,[†,‡] Chunjie Zhou,[†,‡] Huibiao Liu,[†] Zhishan Bo,[†] and Yuliang Li[*,†]

Beijing National Laboratory for Molecular Sciences, CAS Key Laboratory of Organic Solids, Institute of Chemistry, Chinese Academy of Sciences, Beijing 100190, People's Republic of China, and Graduate University of Chinese Academy of Sciences, Beijing 100190, People's Republic of China

Received: July 29, 2009; Revised Manuscript Received: November 4, 2009

Three new hydrogen bonding [60]methanofullerenes (PCB-*t*-BA, PCB-*n*-BA, and MPCB-*t*-BA) are synthesized, characterized, and presented for measurement of the photovoltaic properties. In comparison with the PCBM molecule, the ester group was substituted with *n*-butyric or *t*-butyric alkyl group in the two compounds. Bulk heterojunction (BHJ) organic photovoltaic devices (OPV) employing the methanofullerenes as acceptor were fabricated and optimized. An improvement of power conversion efficiencies (ηe) was observed upon application in P3HT/PCB-n-BA ($\eta e = 0.78\%$) BHJ OPV compared to P3HT/PCBM ($\eta e = 0.59\%$) without thermal annealing with the ratio of 1:1 by weight.

Introduction

Organic solar cells have been attracting much attention around the world within recent years. Organic photovoltaic devices (OPVs) are considered the most promising fossils fuels alternatives due to their possibility to create low-cost, flexible, extremely light solar cells and photodetectors. Since Heeger et al. made the first bulk heterojunction (BHJ) prototype of polymer photovoltaic cells in 1995,[1] the power conversion efficiency has been much improved,[2] in which the active layer consists of a blend of electron-donating materials, for example, *p*-type conjugated polymers and electron-accepting materials (*n*-type). Fullerene derivatives, attributed to their excellent electron-accepting capability, were the best currently available acceptors for BHJ composite; PCBM ([6,6]-phenyl C_{61}-butyric acid methyl ester) was the most widely used methanofullerene as a standard reference acceptor. With an optimized level tuning, band gap, and balanced mobility, organic solar cells can reach power conversion efficiencies about 11%.[3] Many works were done to attain efficiency approaching the magic 10%.[4]

Several factors are important in further improving the power conversion efficiencies (PCE) of BHJ devices, such as UV−vis absorption, highest-occupied molecular orbitals (HOMO), lowest-unoccupied molecular orbitals (LUMO), and band gap relations between the donor and the acceptor, and physical interaction between the donor and the acceptor, manifested by the morphology of active layer.[5] The ideal BHJ solar cell is defined as a bicontinuous composite of donor and acceptor with a maximum interfacial area for exciton dissociation and a mean domain size commensurate with the exciton diffusion length (5−10 nm). The two components should phase separate on a suitable length scale to allow maximum ordering within each phase and thus effective charge transport in continuous pathways to the electrodes so as to minimize the recombination of free charges.[5]

Replacement of PCBM in bulk heterojunction photovoltaic devices was rare.[6] Only the dihydronaphthylfullerene has thus far been reported to give performance commensurate with PCBM.[6d] Substitution of the fullerene derivatives with a variety of solubilizing groups has only induced small changes in the electronic structure. Therefore, the focus has been to optimize the solubilizing group to develop the right level of phase separation with the specific polymeric donor employed.[5] Herein, analogues of PCBM were designed with the aim of improving phase separation with polymeric donors, especially P3HT. In this kind of compounds the ester group of PCBM was replaced by amide groups, resulting in [6,6]-phenyl C_{61}-butylsaure butyl amide (PCB-*t*-BA, PCB-*n*-BA, MPCB-*t*-BA, Chart 1). The weak intermolular hydrogen bonding (H bonding) between N−H···O=C of amide fullerenes may influence the aggregation of the fullerene and the slight modifications of the phenyl ring may lead to significant changes in its solubility and the morphology of the spin-coated films.

Experimental Section

Materials. All solvents were purified and freshly distilled prior to use according to literature procedures and purification handbook. Commercially available materials were used as received unless noted. NMR spectra were obtained using Bruker Avance 400 or 600 spectrometers. ^{1}H NMR and ^{13}C NMR spectra were calibrated using signals from the solvent and reported downfield from TMS. Infrared spectra were obtained on a Bruker Tensor-27. matrix-assisted laser desorption−ionization time-of-flight (MALDI-TOF) spectra were obtained on a Bruker Biflex III MALDI-TOF spectrometer.

Synthesis and Characterization. Experimental and characterization conditions, synthetic details and concrete data were showed in the Supporting Information. The [6,6]-phenyl C_{61}-butylsaure butyl amide were synthesized according to the method developed by Hummelen et al.[7] (Scheme S1 of Supporting Information). General method for a diazomethane addition to C_{60}: A mixture of hydrazono (1 mmol), freshly prepared sodium methoxide (1 mmol) and dry pyridine (15 mL)

* To whom correspondence should be addressed. E-mail: ylli@iccas.ac.cn; liyj@iccas.ac.cn.
† Beijing National Laboratory for Molecular Sciences.
‡ Graduate University of Chinese Academy of Sciences.

10.1021/jp907240n
Published on Web 12/02/2009

CHART 1: Structures of PCBM, PCB-*t*-BA, PCB-*n*-BA, and MPCB-*t*-BA

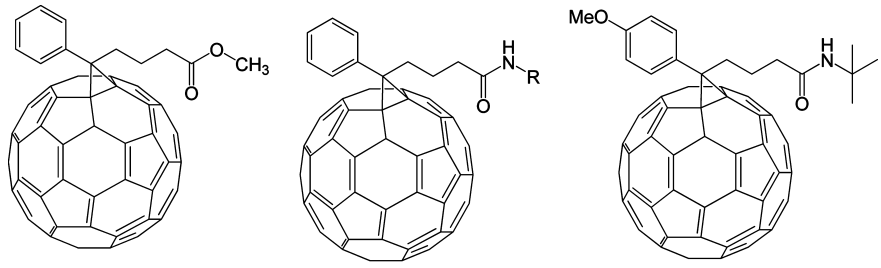

PCBM R= n-butyl PCB-t-BA t-butyl PCB-n-BA MPCB-t-BA

was placed under nitrogen and stirred at room temperature for 30 min. Then a solution of C_{60} (1 mmol) in 1,2-dichlorobenzene (oDCB) (50 mL) was added. The mixture was stirred at 80 °C for 12−24 h and then removed solvent in vacuo. The crude product was chromatographed on silica gel by 0−50% ethyl acetate in toluene as eluent. The mono portion was collected and then resolved in oDCB and refluxed for 24 h to ensure completely change from [5,6] open shell to [6,6] close shell methanofullerenes. After the removal of oDCB in vacuo, the product was precipitated with MeOH, centrifuged, and decanted. The remaining pellet was washed twice with methanol and then dried under vacuo at 100 °C for 24 h, resulting in [6,6]-phenyl C_{61}-butylsaure *t*-butyl amide (PCB-*t*-BA), [6,6]-phenyl C_{61}-butylsaure *n*-butyl amide (PCB-*n*-BA), and (4-methoxyl)phenyl [6,6]-C_{61}-butylsaure *t*-butyl amide (MPCB-*t*-BA)) (Chart 1). The signals for the fullerene sp^2 carbons at 80.4 ppm (PCB-*t*-BA), 78.9 ppm (PCB-*n*-BA), and 80.4 ppm (MPCB-*t*-BA) in ^{13}C NMR spectra indicate C_s symmetry. MALDI-TOF-MS gave the M^+, according to the calculated value of *m*/*z* of all the synthesized C_{60} derivatives. The FT-IR spectra showed absorption features at 1642 cm^{-1} (PCB-*t*-BA), 1641 cm^{-1} (PCB-*n*-BA), and 1647 cm^{-1} (MPCB-*t*-BA) indicating the amide bond and 526 cm^{-1} indicating the fullerene core. The FT-IR spectra showed absorption features at 3301 cm^{-1} (PCB-*t*-BA), 3322 cm^{-1} (PCB-*n*-BA), and 3325 cm^{-1} (MPCB-*t*-BA) and weak absorption at 3490−3400 cm^{-1} indicative a distinct shift to lower frequencies due to H bonding in solid state. The detailed proving of H bonding existence inter the amide fullerenes was showed in the Supporting Information.

(4-Methoxyl)phenyl [6,6]-C_{61}-butylsaure *t*-Butyl Amide (4a). ^1H NMR ($CDCl_3$, 400 MHz) δ (ppm): 7.83 (d, $J = 8.42$ Hz, 2 H), 7.05 (d, $J = 8.44$ Hz, 2 H), 5.26 (s, NH), 3.90 (s, 3 H), 2.85 (t, $J = 7.91$ Hz, 2 H), 2.29 (t, $J = 7.46$ Hz, 2 H), 2.20 (m, 2 H), 1.36 (s, 9 H). ^{13}C NMR ($CDCl_3$, 100 MHz) δ (ppm): 172.0, 159.3, 149.1, 148.2, 146.1, 145.3, 145.3, 145.2, 145.2, 145.0, 144.9, 144.8, 144.8, 144.6, 144.5, 144.1, 143.9, 143.2, 143.2, 143.1, 143.0, 142.4, 142.4, 142.3, 142.2, 141.7, 140.9, 138.2, 133.4, 128.4, 114.0, 80.4 (bridgehead C), 55.51, 51.66, 51.42, 37.35, 33.99, 29.02. IR (KBr) = υ (cm^{-1}): 3325 (m), 2957 (m), 2923 (m), 1647 (s), 1611 (m), 1541 (m), 1511 (s), 1453 (m), 1428 (m), 1250 (s), 1178 (m), 1155 (m), 1107 (w), 1031 (m), 827 (m), 802 (m), 554 (m), 526 (s). MALDI-TOF *m*/*z* 0.981.5 (M^-); calcd. ($C_{75}H_{21}NO$), 981.17.

[6,6]-Phenyl C_{61}-butylsaure *t*-Butyl Amide (4b). ^1H NMR ($CDCl_3$, 600 MHz) δ (ppm): 7.98 (d, $J = 7.22$ Hz, 2 H), 7.56 (t, $J = 7.40$ Hz, 2 H), 7.45 (t, $J = 7.14$ Hz, 1 H), 5.08 (s, 1 H), 1.90 (t, $J = 7.20$ Hz, 2 H), 1.605 (m, 2 H), 1.40 (m, 2 H), 1.37 (s, 9 H). ^{13}C NMR ($CDCl_3$, 100 MHz) δ (ppm): 167.0, 147.8, 146.9, 144.9, 144.1, 144.1, 144.0, 144.0, 143.8, 143.7, 143.6, 143.6, 143.4, 143.4, 143.0, 142.7, 142.1, 142.0, 142.0, 141.9, 141.2, 141.2, 141.1, 141.1, 140.0, 139.71, 136.5, 135.8, 131.2, 127.4, 127.3, 78.9, 70.8, 51.0, 37.7, 36.2, 29.5. IR (KBr) = υ (cm^{-1}): 3301 (m), 2958 (s), 2924 (s), 2867 (m), 1726 (m), 1642 (s), 1547 (m), 1450 (s), 1428 (m),1282 (m), 1262 (m), 1121 (m), 1075 (m), 801 (m), 756 (m), 700 (m), 573 (w), 550 (w), 526 (s). MALDI-TOF *m*/*z* 951.4(M^-); calcd. ($C_{75}H_{21}NO$), 951.96.

[6,6]-Phenyl-C_{61}-butylsaure *n*-Butyl Amide (4c). ($CDCl_3$, 400 MHz) δ (ppm): 7.93 (d, $J = 7.75$ Hz, 2 H), 7.54 (t, $J = 7.70$ Hz, 2 H), 7.47 (t, $J = 6.98$ Hz, 1 H), 5.40 (s, 1 H), 3.25 (q, $J = 6.65$ Hz, 2 H), 2.90 (t, $J = 8.00$ Hz, 2 H), 2.35 (t, $J = 7.37$ Hz, 2 H), 2.207 (m, 2 H), 1.48 (m, 2 H), 1.342 (m, $J = 7.46$ Hz, 2 H), 0.926 (t, $J = 7.28$ Hz, 3 H). ^{13}C NMR ($CDCl_3$, 100 MHz) δ (ppm): 172.0, 159.3, 149.1, 148.2, 146.1, 145.3, 145.3, 145.2, 145.2, 145.0, 144.9, 144.8, 144.8, 144.6, 144.5, 144.1, 143.9, 143.2, 143.2, 143.1, 143.0, 142.4, 142.4, 142.3, 142.2, 141.7, 140.9, 138.2, 137.8, 133.4, 128.4, 114.0, 80.4, 55.5, 51.7, 51.4, 37.4, 34.0, 29.0. IR (KBr) = υ (cm^{-1}): 3322 (m), 2954 (m), 2926 (m), 2864 (m), 1641 (s), 1545 (m), 1494 (w), 1447 (m), 1428 (m), 1377 (m), 1261 (w), 1185 (m), 1160 (m), 1074 (w), 1025 (w), 799 (m), 698 (m), 586 (m), 573 (m), 550 (m), 526 (s). MALDI-TOF CCA *m*/*z* 951.5(M^-); calcd. ($C_{75}H_{21}NO$), 951.96.

UV−Vis, Cyclic Voltammetry, and Thermal Analysis. UV−vis spectra were recorded using JASCO V-570 spectrophotometer in toluene solution. Cyclic voltammetry data were recorded by CHI 660b. The C_{60} derivatives were studied by cyclic voltammetry at 30 °C in oDCB solutions. The reduction potential values are 0.5 ($E_{pa} + E_{pc}$) in V vs ferrocene (Fc)/Fc^+; 10^{-4} to 10^{-3} M in oDCB solution; $TBAPF_6$ (tetrabutyl ammonium hexafluorophosphate 0.1 M) was used as supporting electrolyte, Pt wire as counterelectrode, Ag wire as reference electrode, and glassy carbon as work electrode; a scan rate of 10 mV/s was used; room temperature was ∼30 °C. Differential scanning calorimetry (DSC) data were recorded by PerkinElmer Diamond DSC (N536−0022) F.T.; thermal gravity analysis (TGA) data were recorded by Shimadzu DTG-60; samples were kept at 100 °C in vacuo for 24 h before thermal analysis.

Device Fabrication and Photovoltaic Characterization. The typical device structure used in this study was a sandwich structure with ITO/PEDOT as a hole-collecting electrode and Al as an electron-collecting electrode. In the structure of the devices, the active layer has a thickness of 100 nm, as determined by surface profilometer (Tencor, ALFA-Step 500). Indium/tin oxide (ITO) was used as the anode and a 50-nm thick poly (ethylene dioxythiophene)/polystyrenesulfonic acid (PEDOT-PSS, Batron-P, Bayer AG) layer was incorporated between the ITO and the active layer to reduce device leakage. Methanofullerenes as acceptor were dissolved in oDCB solution. P3HT (Aldrich) was dissolved in oDCB solution. Both solutions

TABLE 1: Electrochemical Data

compounds	E^1_{red}	E^2_{red}	E^3_{red}
C_{60}	−1.120	−1.512	−1.982
PCBM	−1.175	−1.553	−2.058
PCB-*t*-BA	−1.167	−1.535	−2.036
PCB-*n*-BA	−1.167	−1.536	−2.036
MPCB-*t*-BA	−1.168	−1.536	−2.052

were mixed to give the calculated weight ratio of donor material to acceptor material, while the solution for the third type of cells was added with extra 2.5% 1,12-diiodododecane (DI_2) by weight. The blend solution was spin coated onto the top of PEDOT-PSS. Finally, Parts of cells were thermally evaporated onto the top of the photoactive polymer blend. The deposition rates and the thickness of the evaporation layers were monitored by a thickness/rate meter (Sycon). The deposition rates for aluminum were usually 0.01−0.02 nm/s. The crossing area between the cathode and the anode define the sensing area. Unless otherwise specified, 0.04 cm^2 active area was typically used in this study. All the fabrication steps were carried out in a nitrogen glovebox. The I−V characteristics in the dark and under illumination were measured with a Keithley 236 source-measure unit. Photocurrent was measured under a solar simulator with AM 1.5 illumination (100 mW/cm^2) under atmosphere.

Atomic Force Microscopy (AFM), Optical Microscope (OM), and Scanning Electronic Microscopy Energy-Dispersive Spectrometry (SEM-EDS). AFM measurements were carried out with Multimode Nanoscope controller IIIa (Veeco Inc.) operated in tapping mode. OM data were recorded by Nikon eclipe E600 and Nikon E4500. SEM images were taken with Hitachi S-4300 or Hitachi S-4800. EDS data were obtained by Hitachi S-4800.

Results and Discussions

Electrochemical Properties. All four C_{60} derivatives showed similar cyclic voltammograms with three quasireversible reduction waves in the potential ranging from −0.3 to −2.0 V. Reduction potentials were listed in Table 1. The reduction potentials of methanofullerene derivatives are shifted to more negative values with respect to C_{60} because of the decrease of the number of π electrons and the release of strain energy.[8] It was reported that the attached reductive group influences the redox property of [60]fullerene derivatives.[9] The reduction potential of PCB-*t*-BA and PCB-*n*-BA are almost same, because of similar structure and no electron push or pull group difference; methoxy groups in the para position of the phenyl ring can lead to a slightly decrease of the reduction potential.[4c,9] The reduction potentials of these amide fullerenes are slightly positive than that of PCBM.

UV−Vis Measurement. The UV−vis spectra of the fullerene derivatives compared with that of the pure C_{60} in toluene solution was shown in Figure 1. The amide derivatives showed sharp peak at 434 nm, 1 nm red-shift compared with that of PCBM. Broad peaks ranging from 450 to 650 nm were also observed. The absorption at 696 nm for PCB-*t*-BA, 697 nm for PCB-*n*-BA, and MPCB-*t*-BA are specific to [6,6] addition in C_{60} core. It is noted that the absorption profiles for the amide derivatives are very close to that of PCBM. The results showed that there is no dramatic change in the band structure for the amide derivatives as consistent with the analogical structures, meanwhile convincing the analogue of E^1_{red}.

TGA. TGA (see Figure S3 of Supporting Information) and DSC of four fullerene derivatives were measured to understand the thermal stability of the fullerene derivatives. TGA results

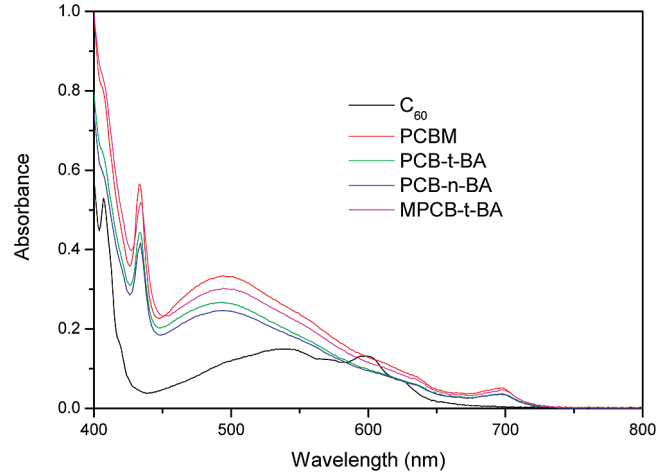

Figure 1. Normalized UV−vis absorbance spectra of fullerene derivatives in toluene.

indicate that all fullerene derivatives have a thermal decomposition temperature higher than 250 °C. The DSC measurement of PCBM molecule shows a crystallization peak at 280 °C, without any other transition between 20 and 340 °C. However, no crystallization or glass transitions (T_g) were observed in the curves of other methanofullerenes between 20 and 280 °C, which suggests that they are amphorous materials.[10]

Organic Photovoltaic Devices Performance. The performance of photovoltaic devices of P3HT/fullerene was investigated using classical ITO/PEDOT:PSS/P3HT:fullerenes/Al structure. To optimize the photovoltaic devices, we have successfully fabricated three classes of devices. Figure 2 showed a comparison of the *JV* curves of PCB-*t*-BA, PCB-*n*-BA, MPCB-*t*-BA, and PCBM-based BHJ devices with three cell conditions.

First, we fabricated cells with the ratio of 1:4 for P3HT:fullerene by weight. The performance was much lower than we expected, showed in Figures 2a and 3. The cell performance of no-annealing and postanneal was different, the highest PCE (0.45%) of MPCB-*t*-BA was slightly higher than that 0.42% of PCBM, whose phase segregation scale were analogous. However, anneal thoroughly destroyed the active layer composed of P3HT and amide fullerene with PCE of almost zero, while PCBM achieved 1.55%. OM in Figure 4 showed there were plenty of amide fullerene crystals on the surface of active layer when the devices were annealed, which means the phase separation was fairly large-scaled and contributed to inefficient charge transfer and separation. AFM in Figure 5, AFM section analysis in Figure S4 of Supporting Information, and SEM-EDS in Figure S6 of Supporting Information also verified[11] the aggregation with size up to hundreds of micrometers in length, two to ten micrometers in width, and several hundred nanometers in height; the aggregation was attributed to the strong H bonding between amide fullerene.

To resolve the large-scale phase separation and serious aggregations of amide fullerenes, we decreased the proportion of fullerene to 1:1 as suggested by Manca et al.[11] We found that the cell performance of the no-annealing cell of amide fullerenes and PCBM increased, and PCB-*n*-BA's performance (0.78%) was higher than PCBM (0.59%). *JV* curves, PCE, and Voc were shown in Figures 2b, 3, and 4; AFM images were shown in Figure S5 of Supporting Information .Hydrogen bonding assembly is a good way to fabrication of molecular arrays and shapes for efficient intermolecular energy and electron transfer between donor and acceptor units due to its high selectivity and directionality.[12] The uniform and order

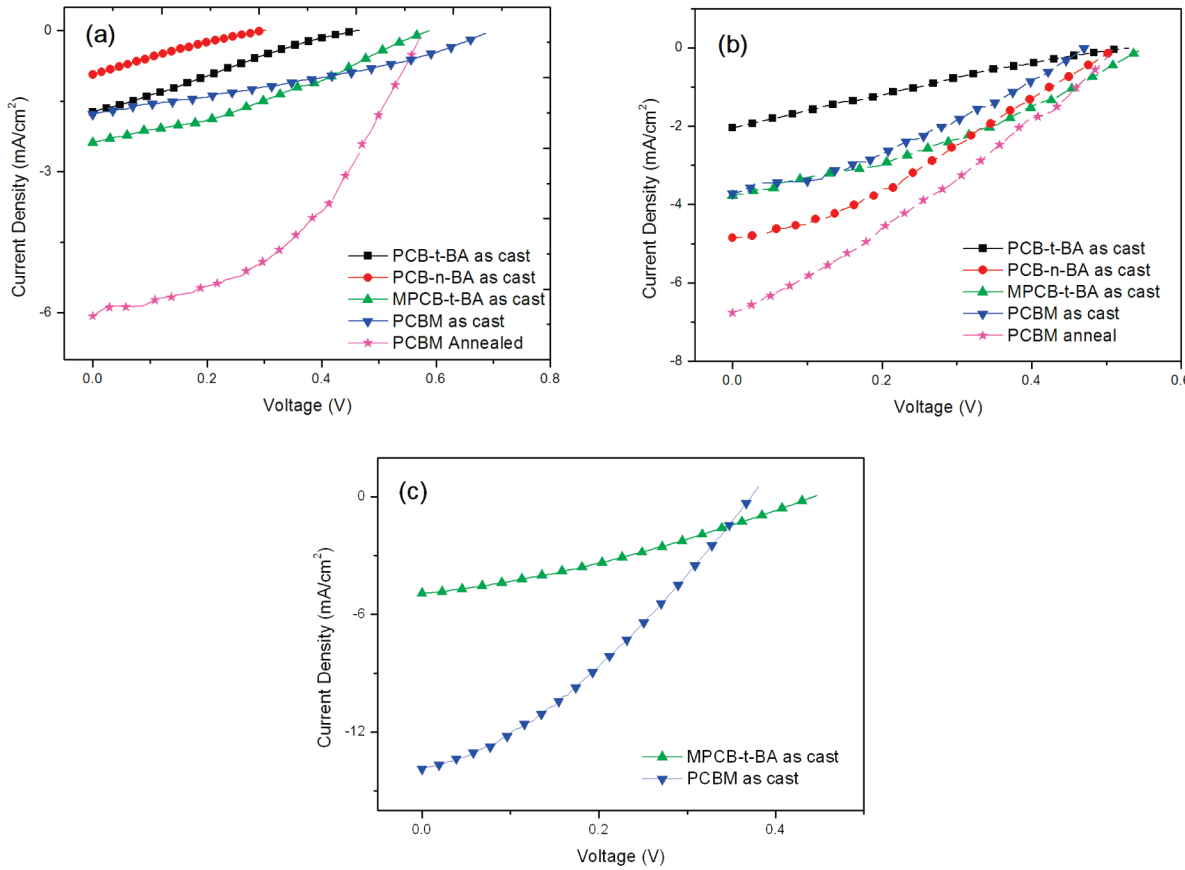

Figure 2. The *JV* curves of PCB-*t*-BA, PCB-*n*-BA, MPCB-*t*-BA, and PCBM-based BHJ devices under AM1.5 illumination at 100 mW/cm^2. (a) P3HT:fullerene = 1:4; (b) P3HT:fullerene = 1:1; (c) P3HT:fullerene = 1:4 with 2.5% DI_2; all ratios were based on weight.

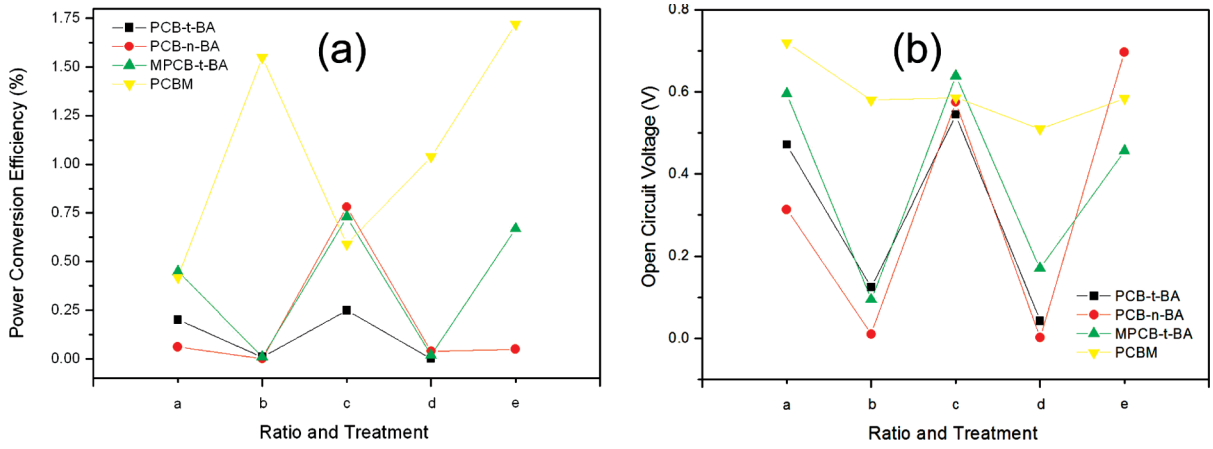

Figure 3. (a) PCE of each type of cells; (b) OCV of each type of cells. Cell conditions: (a) P3HT:fullerenes = 1:4 as cast; (b) P3HT:fullerenes = 1:4 annealed; (c) P3HT:fullerenes = 1:1 as cast; (d) P3HT:fullerenes = 1:1 annealed; (e) P3HT:fullerenes = 1:4 as cast with 2.5% DI_2; all ratios were based on weight.

morphology of the polymer:fullerene is an important factor to higher power conversion efficiencies.[5,13] The calculation studies also showed that the self-assembly of PCBM on the gold surface was mainly controlled by weak hydrogen bonding between the PCBM tails.[14] Although PCBM is a crystallizable molecule, it is very difficult to nucleate homogeneously within the whole film to form nanoscale crystals. Consequently, the composite film is either very homogeneous without obvious phase separation or PCBM crystallizes into crystals with several micrometers upon conventional thermal annealing, leading to large-scale phase separation in the film.[15] In our case, the amide hydrogen bonding can help the fullerene moiety to stack as homogeneous and order domain in the photoactive layer so as to create short and continuous pathways for electron transport. So hydrogen bonding interaction can results in the molecular aggregates orderly for improving the performance of the resulted devices. However, with thermal annealing, the strong amide hydrogen bonding interaction can lead to large-scale phase separation and the PCE of the postannealing amide fullerene cell increased slightly from 0 to 0.04%, which was much lower than 1.04% of PCBM. AFM

By addition of a few volumes of alkanedithiols or halogenalkanes in the solution used to spin-cast films comprising of polymer and fullerene derivatives, the cell performance may be increased obviously through altering the bulk heterojunction morphology, which enable morphological control in active layer

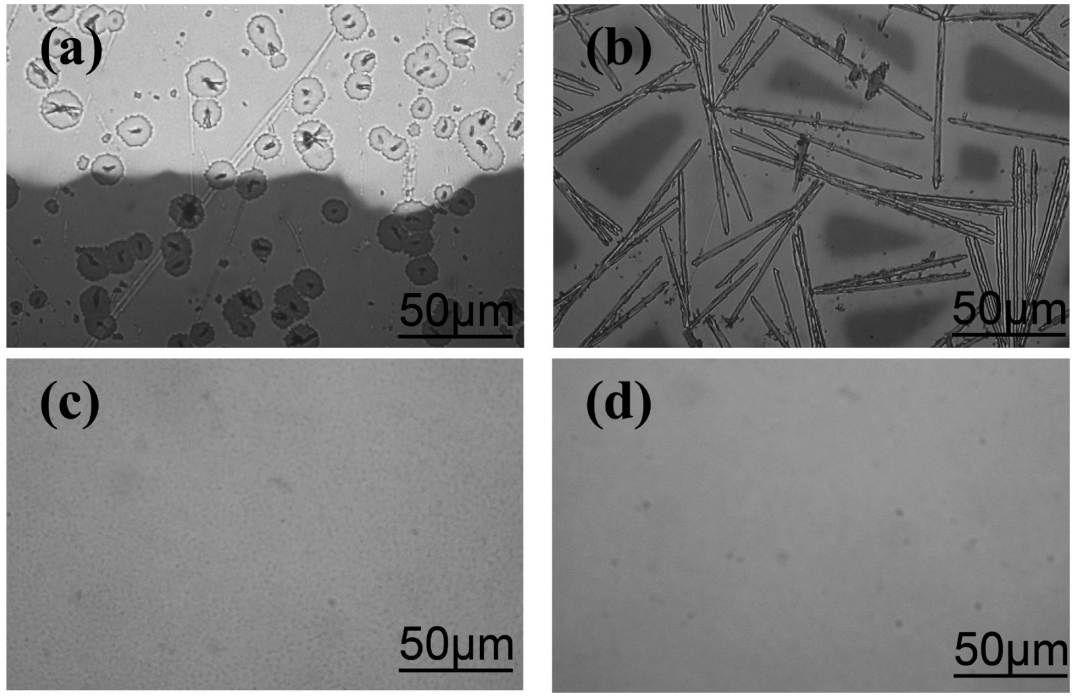

Figure 4. OM of four typical morphology on the surface of BHJ solar cell. (a) P3HT:PCB-*n*-BA = 1:4 with DI_2 as cast; (b) P3HT:PCB-*n*-BA = 1:4 annealed; (c) P3HT:PCB-*n*-BA = 1:1 as cast; (d) P3HT:PCBM = 1:4 with DI_2 as cast.

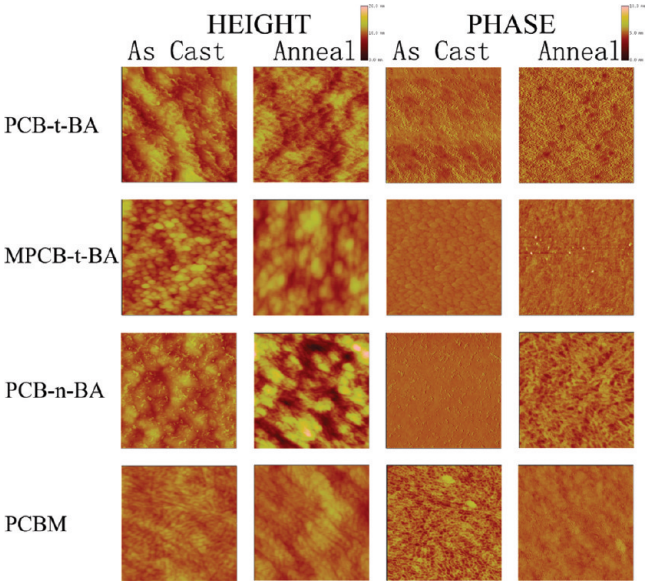

Figure 5. AFM topology images (500 nm × 500 nm) of films cast from oDCB solution with the ratio of 1:4 of P3HT: fullerenes by weight.

when thermal annealing is either undesirable or ineffective.[16] As annealing was ineffective to amide fullerenes, we tried to add 2.5% of DI_2 to the mixed solution whose weight ratio was 1:4 with the ratio of 1:4 of P3HT:fullerenes by weight. Unfortunately, the cell performance of amide fullerene derivatives was not improved while PCBM achieved the highest efficiency of 1.77%, which suggested that DI_2 did not restrain the strong aggregation trend of amide methanofullerenes leading to big-scale phase separation, revealed by an AFM image in Figure S7 of Supporting Information.

Conclusions

The synthesis, characterization, and application of three new amide [60]methanofullerenes (PCB-*t*-BA, PCB-*n*-BA, and MPCB-*t*-BA) as new acceptors in BHJ solar cells were discussed. The power conversion efficiency was measured of P3HT/PCB-*n*-BA without thermal annealing to show a value of $\eta_e = 0.78\%$. The bulk heterojunction photovoltaic cells of P3HT/PCBM were also fabricated for comparison (0.59%). P3HT/PCB-*n*-BA showed a significant improvement in power conversion efficiencies. The result indicates that the hydrogen-bonding interaction can results in the molecular aggregates orderly for improving the performance of the resulted devices.

Acknowledgment. This work was supported by the National Nature Science Foundation of China (20531060, 20831160507, and 10874187) and the National Basic Research 973 Program of China.

Supporting Information Available: Synthetic details, supporting data, tables and figures. This material is available free of charge via the Internet at http://pubs.acs.org.

References and Notes

(1) Yu, G.; Gao, J.; Hummelen, J. C.; Wudl, F.; Heeger, A. J. *Science* **1995**, *270* (5243), 1789–1791.

(2) (a) Li, G.; Shrotriya, V.; Huang, J. S.; Yao, Y.; Moriarty, T.; Emery, K.; Yang, Y. *Nat. Mater.* **2005**, *4* (11), 864–868. (b) Peet, J.; Kim, J. Y.; Coates, N. E.; Ma, W. L.; Moses, D.; Heeger, A. J.; Bazan, G. C. *Nat. Mater.* **2007**, *6* (7), 497–500. (c) Ma, W. L.; Yang, C. Y.; Gong, X.; Lee, K.; Heeger, A. J. *Adv. Funct. Mat.* **2005**, *15* (10), 1617–1622. (d) Yip, H. L.; Hau, S. K.; Baek, N. S.; Ma, H.; Jen, A. K. Y. *Adv. Mater.* **2008**, *20* (12), 2376–2382. (e) Irwin, M. D.; Buchholz, B.; Hains, A. W.; Chang, R. P. H.; Marks, T. J. *Proc. Natl. Acad. Sci. U.S.A.* **2008**, *105* (8), 2783–2787.

(3) Koster, L. J. A.; Mihailetchi, V. D.; Blom, P. W. M. *Appl. Phys. Let.* **2006**, *88* (9), 093511.

(4) (a) Riedel, I.; Martin, N.; Giacalone, F.; Segura, J. L.; Chirvase, D.; Parisi, J.; Dyakonov, V. *Thin Solid Films* **2004**, *451*−*452*, 43–47. (b) Zheng, L.; Zhou, Q.; Deng, X.; Yuan, M.; Yu, G.; Cao, Y. *J. Phys.Chem. C* **2004**, *108* (32), 11921–11926. (c) Kooistra, F. B.; Knol, J.; Kastenberg, F.; Popescu, L. M.; Verhees, W. J. H.; Kroon, J. M.; Hummelen, J. C. *Org. Lett.* **2007**, *9* (4), 551–554. (d) Pavel, A.; Troshin, H. H.; Renz, J.; Egginger, M.; Mayorova, J. Yu.; Goryachev, A. E.; Peregudov, A. S.;

Lyubovskaya, R. N.; Gobsch, G.; Sariciftci, N. S.; Razumov, V. F. *Adv. Funct. Mat.* **2009**, *19* (5), 779–788.

(5) Thompson, B. C.; Frechet, J. M. J. *Angew. Chem., Int. Ed.* **2008**, *47* (1), 58–77.

(6) (a) Lacramioara, M. P.; Patrick van't, H.; Alexander, B. S.; Harry, T. J.; Jan, C. H. *Appl. Phys. Let.* **2006**, *89* (21), 213507. (b) Riedel, I.; von Hauff, E.; et al. *Adv. Funct. Mat.* **2005**, *15* (12), 1979–1987. (c) Lenes, M.; Wetzelaer, G. J. A. H.; Kooistra, F. B.; Veenstra, S. C.; Hummelen, J. C.; Blom, P. W. M. *Adv. Mater.* **2008**, *20* (11), 2116. (d) Backer, S. A.; Sivula, K.; Kavulak, D. F.; Frechet, J. M. J. *Chem. Mater.* **2007**, *19* (12), 2927–2929. (e) Kennedy, R. D.; Ayzner, A. L.; Wanger, D. D.; Day, C. T.; Halim, M.; Khan, S. I.; Tolbert, S. H.; Schwartz, B. J.; Rubin, Y. *J. Am. Chem. Soc.* **2008**, *130* (51), 17290–17292.

(7) Hummelen, J. C.; Knight, B. W.; LePeq, F.; Wudl, F.; Yao, J.; Wilkins, C. L. *J. Org. Chem.* **1995**, *60* (3), 532–538.

(8) Haddon, R. C. *Science* **1993**, *261* (5128), 1545–1550.

(9) Suzuki, T.; Maruyama, Y.; Akasaka, T.; Ando, W.; Kobayashi, K.; Nagase, S. *J. Am. Chem. Soc.* **1994**, *116* (4), 1359–1363.

(10) Zhang, Y.; Yip, H.-L.; Acton, O.; Hau, S. K.; Huang, F.; Jen, A. K. Y. *Chem. Mater.* **2009**, *21*, 2598–2600.

(11) Swinnen, A.; Haeldermans, I.; vande Ven, M.; D'Haen, J.; Vanhoyland, G.; Aresu, S.; D'Olieslaeger, M.; Manca, J. *Adv. Funct. Mat.* **2006**, *16* (6), 760–765.

(12) (a) Prins, L. J.; Reinhoudt, D. N.; Timmerman, P. *Angew. Chem., Int. Ed.* **2001**, *40* (13), 2382–2426. (b) Schenning, A. P. H. J.; von Herrikhuyzen, J.; Jonkheijm, P.; Chen, Z.; Wurthner, F.; Meijer, E. W. *J. Am. Chem. Soc.* **2002**, *124* (35), 10252–10253. (c) Berg, A.; Shuali, Z.; Asano-Someda, M.; Levanon, H.; Fuhs, M.; Mobius, K. *J. Am. Chem. Soc.* **1999**, *121* (32), 7433–7434. (d) Guldi, D. M.; Martin, N. *J. Mater. Chem.* **2002**, *12* (7), 1978–1992. (e) Liu, Y.; Zhuang, J. P.; Liu, H. B.; Li, Y. L.; Lu, F. S.; Gan, H. Y.; Jiu, T. G.; Wang, N.; He, X. R.; Zhu, D. B. *Chemphyschem* **2004**, *5* (8), 1210–1215.

(13) (a) Yang, X. N.; Loos, J.; Veenstra, S. C.; Verhees, W. J. H.; Wienk, M. M.; Kroon, J. M.; Michels, M. A. J.; Janssen, R. A. J. *Nano Lett.* **2005**, *5* (4), 579–583. (b) Yang, C. Y.; Hu, J. G.; Heeger, A. J. *J. Am. Chem. Soc.* **2006**, *128* (36), 12007–12013.

(14) Wang, Y.; Alcami, M.; Martin, F. *Chemphyschem* **2008**, *9* (7), 1030–1035.

(15) Li, L. G.; Lu, G. H.; Li, S. J.; Tang, H. W.; Yang, X. N. *J. Phys. Chem. B* **2008**, *112* (49), 15651–15658.

(16) (a) Peet, J.; Soci, C.; Coffin, R. C.; Nguyen, T. Q.; Mikhailovsky, A.; Moses, D.; Bazan, G. C. *Appl. Phys. Let.* **2006**, *89*, 252105. (b) Peet, J.; Kim, J. Y.; Coates, N. E.; Ma, W. L.; Moses, D.; Heeger, A. J.; Bazan, G. C. *Nat. Mater.* **2007**, *6* (7), 497–500.

JP907240N